PCCP

Accepted Manuscript




ROYAL SOCIETY OF CHEMISTRY

www.rsc.org/pccp

ARTICLE TYPE www. rsc.org/xxxxxx | XXXXXXXX

# Development of a ReaxFF potential for Pt/O systems describing the energetics and dynamics of Pt-oxide formation†

**Donato Fantauzzi,[a] Jochen Bandlow,[a] Lehel Sabo,[a] Jonathan E. Mueller,[a] Adri C. T. van Duin,[b] and Timo Jacob*[a]**

***Received Xth XXXXXXXXXX 20XX, Accepted Xth XXXXXXXXX 20XX***
***First published on the web Xth XXXXXXXXXX 200X***
**DOI: 10.1039/b000000x**

ReaxFF force field parameters describing Pt-Pt and Pt-O interactions have been developed and tested. The Pt-Pt parameters are shown to accurately account for the chemical nature, atomic structures and other materials properties of bulk platinum phases, low and high-index platinum surfaces and nanoclusters. The Pt-O parameters reliably describe bulk platinum oxides, as well as oxygen adsorption and oxide formation on Pt(111) terraces and the {111} and {100} steps connecting them. Good agreement between the force field and both density functional theory (DFT) calculations and experimental observations is demonstrated in the relative surface free energies of high symmetry Pt-O surface phases as a function of the oxygen chemical potential, making ReaxFF an ideal tool for more detailed investigations of more complex Pt-O surface structures. Validation for its application to studies of the kinetics and dynamics of surface oxide formation in the context of either molecular dynamics (MD) or Monte Carlo simulations are provided in part by a two-part investigation of oxygen diffusion on Pt(111), in which nudged elastic band (NEB) calculations and MD simulations are used to characterize diffusion processes and to determine the relevant diffusion coefficients and barriers. Finally, the power of the ReaxFF reactive force field approach in addressing surface structures well beyond the reach of routine DFT calculations is exhibited in a brief proof-of-concept study of oxygen adsorbate displacement within ordered overlayers.

## 1 Introduction

Late transition metals play an important role in heterogenous and electro-catalysis, where they are utilized in a wide range of industrial processes. Because transition metals often exhibit varying affinities for oxygen, the presence of oxygen in the catalytic environment can strongly affect the catalysts' actual structure and chemical composition. Different metal oxygen surface states (*e.g.* adsorbed oxygen, surface oxide films, and bulk metal oxides) have been shown to exhibit different catalytic properties in studies of transition metal catalysts including Ru [1–4], Ag [5–7], Pd [8–11] and Pt [12–15]. Therefore, the performance of a transition metal catalyst can depend sensitively on the extent of oxidation, the associated surface morphology and electronic structure, and hence on the catalytic environment. Furthermore, because the characterization of catalytically active surface structures is often technologically challenging and scientifically intriguing, it continues to be an area of active scientific investigation.

Platinum has captured an exceptional position among the transition metals in heterogenous catalysis, not only for it's numerous applications (*e.g.* in catalytic converters in automobiles [16,17], in polymer electrolyte fuel cells (PEMFC's) as electrode material [18–20], *etc.*), but also for the extensive treatment it has received in surface science and electrochemistry from both experimental and theoretical points of view.

Although platinum nanoparticles are often employed in these applications, these studies have typically investigated a single elementary process (*e.g.* oxygen adsorption, desorption, dissociation, or diffusion) on idealized, high-symmetry surfaces [21–44], to simplify the analysis of experimental results and to make the problem tractable for *ab-initio* methods. Among the low-index platinum surfaces, Pt(111) has received particular attention, due to its high thermodynamic stability and expected dominance on real catalyst surfaces. These studies have been carried out with the hope of gaining insights into the performance of real catalysts, however, realistic catalysts– and even model single-crystal surfaces– are not defect-free, but include low-coordination surface sites (*e.g.* step edges, kinks, *etc.*). More recently low-coordination surface sites are being investigated by studying vicinal surfaces and surfaces with other types of regular defects, with the aim of developing

† Electronic Supplementary Information (ESI) available: Computational details, the developed ReaxFF Pt/O force field parameters as well as the ReaxFF and DFT-PBE obtained structures and energies are provided. See DOI: 10.1039/b000000x/

[a] *Institut für Elektrochemie, Universität Ulm, Albert-Einstein-Allee 47, D-89069 Ulm, Germany. Fax: +49 (0) 731 50 25469 ; Tel: +49 (0) 731 50 25400; E-mail: timo.jacob@uni-ulm.de*
[b] *Department of Mechanical and Nuclear Engineering, Pennsylvania State University, University Park, PA 16801, USA.*

a systematic understanding of the influence of defects. These studies represent the advent of methods to bridge the so-called materials gap between real and model catalysts.

While researchers have begun to study these more complex surface structures, there are still a number of unresolved questions related to high-oxygen-coverage states in the oxidation of Pt(111). At low coverages of surface oxygen, experiments and theoretical calculations paint a consistent picture of the stable surface phases[45,46]. Norton *et al.*[47] used low-energy electron diffraction (LEED) measurements in conjunction with a nuclear microanalysis to show that the adsorption of oxygen from molecular beams on a Pt(111) surface leads to the formation of a $p(2 \times 2)$ oxygen overlayer, with an overall coverage of 0.25 ML. In a scanning tunneling microscopy (STM) study Devarajan *et al.*[48] observed that the exposure of a Pt(111) surface to atomic oxygen leads to (i) a zigzagged $p(2 \times 1)$ oxygen overlayer in coexistence with the $p(2 \times 2)$ oxygen phase for coverages $> 0.25$ ML, (ii) a dominance of the zigzagged $p(2 \times 1)$ overlayer at a coverage of 0.5 ML, and (iii) one-dimensional (1D) Pt-oxide chains, which preserve the $p(2 \times 1)$ symmetry, for coverages $> 0.5$ ML. Hawkins *et al.*[49] were able to model the structure of these Pt-oxide chains and reproduce their stability using density functional theory (DFT). Two structures have been proposed for 1.00 ML coverage. Miller *et al.*[50] used DFT calculations to help interpret their *in-situ* x-ray photoelectron spectroscopy (XPS) and *ex-situ* x-ray absorption spectroscopy (XAS) results to predict an oxide chain structure. Shortly thereafter Holby *et al.*[51] proposed a novel hybrid structure involving place-exchange, which they found to be more stable than previously published structures using DFT calculations.

While they have often raised as many questions as they have answered, DFT calculations have proven to be an invaluable tool to complement surface science experiments in determining surface structures in atomistic detail. Nevertheless, in addition to the materials gap mentioned previously, typical DFT calculations suffer alongside ultra high vacuum (UHV) experiments from the so-called temperature and pressure gap, since technological applications typically require at least ambient temperatures and pressures. While thermodynamic approximations can be used to extend the results of DFT calculations across this temperature and pressure gap, severe limitations on the time and length scales that can be explicitly addressed in DFT calculations make it difficult to move beyond these non-dynamical equilibrium models (*e.g.* using *ab-initio* MD simulations) and render DFT methods incapable of adequately describing important aspects of many experimental systems. In particular, this has barred the way to a fundamental understanding of oxygen's influence on platinum catalysts' morphology and catalytic activity.

To address these deficiencies, we have developed a reactive interaction potential (force field) within the ReaxFF framework[52]. In contrast to nonreactive potentials (*e.g.* EAM[53–56], MEAM[57], UFF[58,59], CHARMM[60], OPLS[61], or AMBER[62,63]) ReaxFF is able to describe chemical reactions (*i.e.* bond formation and dissociation) with almost QM accuracy. While the sophisticated system energy formulation required to describe chemical reactivity makes ReaxFF computationally more demanding than nonreactive potentials, it is still orders of magnitude faster than *ab-initio* methods.

The values for the parameters of the force field presented here were obtained by optimizing them to reproduce an extensive set of energies and geometries obtained from DFT for a variety of structures involving platinum and oxygen. These structures include various bulk platinum phases, oxygen adsorbates at various Pt(111) surface sites and defects, in conjunction with various oxygen coverages, initial stages of Pt(111) surface oxide formation and platinum bulk oxides.

A general description of the ReaxFF methodology along with the *ab-initio* method used to generate the results, against which the force field was optimized, is given in section 2. A detailed description of the Pt/O force field optimization is presented in section 3.1. To validate the suitability of our ReaxFF force field description for studying kinetic aspects of the Pt/O systems within either kinetic Monte Carlo (kMC) or MD simulations, we compare ReaxFF descriptions of oxygen diffusion and displacement processes on Pt(111) with independent DFT calculations and experimental results in section 3.2.

## 2 Methodology

### 2.1 ReaxFF

ReaxFF is a reactive molecular dynamics (MD) method that uses a bond-order-dependent potential energy formulation, in conjunction with time-dependent, polarizable charge descriptions, to continuously describe bond formation and cleavage in a wide range of chemical environments. Like the Tersoff[64] and Brenner[65] potentials, it is based on Pauling's idea of mapping bond distances onto bond orders in order to enable the determination of the different quantum chemical states of a structure[66]. Thus ReaxFF is able to describe electronic-structure-dependent chemical properties of atoms, without containing explicit descriptions of individual electrons. The general form of the ReaxFF potential is:

$$\begin{aligned} E_{\text{system}} &= E_{\text{bond}} + E_{\text{val}} + E_{\text{tors}} + E_{\text{over}} \\ &+ E_{\text{under}} + E_{\text{vdW}} + E_{\text{Coulomb}}, \end{aligned} \quad (1)$$

where $E_{\text{system}}$ is the total potential energy of the system, $E_{\text{bond}}$ is the covalent bond energy, $E_{\text{val}}$ and $E_{\text{tors}}$ are the energies associated with three-body valence angle strains and four-body torsional angle strains, $E_{\text{over}}$ and $E_{\text{under}}$ are energy penalties which enforce valency, and $E_{\text{Coulomb}}$ and $E_{\text{vdW}}$ are the energies associated with electrostatic and dispersive interactions.

The first three energy contributions are functions of the bond-order, which is, in general, defined as:

$$\begin{aligned} BO_{ij} &= BO_{ij}^{\sigma} + BO_{ij}^{\pi} + BO_{ij}^{\pi\pi} \\ &= \exp\left[p_{\mathrm{bo1}}\left(\frac{r_{ij}^{\sigma}}{r_0}\right)^{p_{\mathrm{bo2}}}\right] \\ &+ \exp\left[p_{\mathrm{bo3}}\left(\frac{r_{ij}^{\pi}}{r_0}\right)^{p_{\mathrm{bo4}}}\right] \\ &+ \exp\left[p_{\mathrm{bo5}}\left(\frac{r_{ij}^{\pi\pi}}{r_0}\right)^{p_{\mathrm{bo6}}}\right], \end{aligned} \quad (2)$$

where $BO_{ij}$ is the bond-order between atoms $i$ and $j$, $r_{ij}$ the inter-atomic distance, $r_0$ the equilibrium bond distance, and the $p_{\mathrm{bo}}$ terms are empirical parameters. The dependence of these energy contributions on bond order ensures that the overall system energy is a continuous function of the inter-atomic distances, so that there are no discontinuities as $\sigma$, $\pi$, and $\pi\pi$ bonds or other potential energy contributions vanish or appear. Furthermore, it ensures that the potential energy surface is differentiable, thus enabling direct calculation of inter-atomic forces. For instance, the covalent bond energy is then given by:

$$E_{\mathrm{bond}} = -D_{\mathrm{e}} \cdot BO_{ij} \cdot \exp[p_{\mathrm{be1}}(1-(BO_{ij})^{p_{\mathrm{be2}}})], \quad (3)$$

where $D_{\mathrm{e}}$ corresponds to the bond dissociation energy and the $p_{\mathrm{be}}$ terms are empirical parameters. Electrostatic and dispersive interactions are calculated between all atom pairs regardless of their connectivity. Both terms are directly calculated from the inter-atomic distance, but have no direct dependance on the bond-order. Electrostatic interactions are described via a variable-charge electrostatic description that computes the partial charge of individual atoms using a self-consistent electron equilibration method (EEM) developed by Mortier *et al.*[67]. The full expressions for each of these terms are given and explained in the first publication on the ReaxFF methodology and its application to hydrocarbon chemistry from 2001[52]. Since then the ReaxFF approach has been successfully extended to the treatment of a multitude of other chemical systems, including both metals[68–70] and metal oxides[71–75]. Empirical parameters are obtained by optimizing them, so that ReaxFF is able to reproduce data obtained from higher level *ab-initio* calculations or experiments. The optimization procedure utilizes a successive one-parameter search technique described previously[72,76]. The transferability of the optimized parameters can be validated by testing their ability to reproduce DFT-data not used in the optimization.

### 2.2 DFT

DFT calculations employed SeqQuest[77,78], a periodic DFT code with localized basis sets comprised of linear combinations of Gaussian functions, within the generalized gradient approximation (GGA) exchange-correlation functional developed by Perdew, Burke and Ernzerhof[79] (PBE). A standard (non-local), norm-conserving pseudopotential[80] replaced the 68 core electrons of each Pt atom, leaving the 5*d*- and 6*s*-electrons in the valence space and invoking a nonlinear core correction[81]. Valence electrons were described using optimized, "double-$\zeta$ plus polarization"-type, contracted Gaussian functions. Calculations involving Pt(111) terraces were performed on a seven-layer slab, in which the lowest two layers were fixed to the calculated bulk crystal structure, while the remaining five surface layers were allowed to fully relax to $<$ 0.026 eV/Å. Integrations in reciprocal space were performed using a Brillouin zone (BZ) sampling of 19 $\times$ 19 Monkhorst-Pack $\boldsymbol{k}$-points for the $1\times1$ unit cell, while integrations in real space were performed on a grid spacing of 0.14 Å. The vicinal Pt(111) surfaces were modeled as seven-layer slabs, in which the lowest three layers were fixed to the calculated bulk crystal structure, using a Brillouin zone (BZ) sampling of 5 $\times$ 19 Monkhorst-Pack $\boldsymbol{k}$-points for the $4\times1$ unit cell and a grid spacing of 0.14 Å. Analogous parameters were used for calculating bulk structures.

## 3 Results

### 3.1 Force field development: optimization and validation

#### 3.1.1 Training and transferability of Pt-Pt interactions.

*3.1.1.1 Training of bulk phases.* The force field description of the Pt-Pt interactions was obtained by optimizing the relevant empirical force field parameters so that ReaxFF could reproduce energies and structures for bulk platinum obtained from DFT calculations. These bulk structures included uniform expansions and compressions of face centered cubic (fcc), ideal hexagonal close-packed (hcp), body centered cubic (bcc), simple cubic (sc), diamond (dia), and $\beta$-tungsten ($\beta$W) bulk phases of platinum. Figure 1 shows the equations of state obtained from our ReaxFF force field after the optimization procedure, along with those obtained from the employed DFT-PBE calculations. ReaxFF reproduces the atomic energies ($E_{\mathrm{atom}}$) and volumes ($V_{\mathrm{atom}}$) of the minimum energy structures, along with the curvature near these minima for the low-energy phases. The curves for the hcp phase illustrated in Fig. 1 a) and b), for ReaxFF and DFT-PBE, respectively, were obtained for structures with the idealized *c*/*a* ratio. If instead the optimized *c*/*a* ratio is used ReaxFF predicts that bulk platinum should undergo a phase transition from the fcc phase to the hcp phase, at high pressures. This prediction is in agreement with both experimental observations and theoretical calculations[82]. Deviations for the less stable high-energy phases,

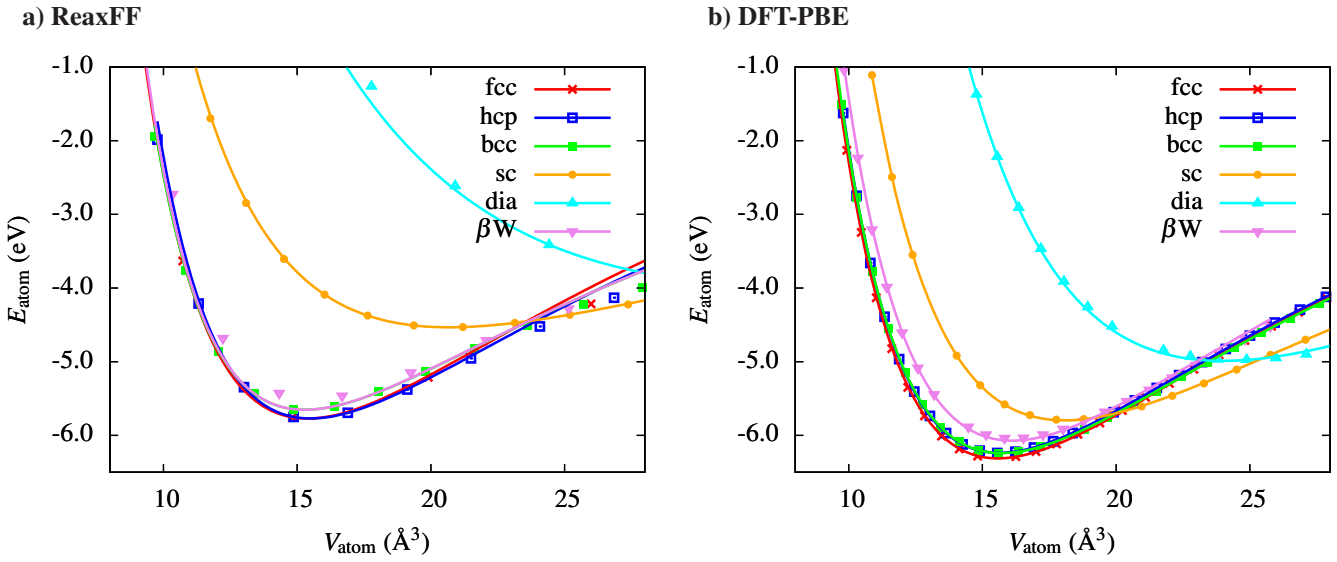


**Fig. 1** Equations of state, using the equations developed by Li *et al.*[83] for bulk platinum structures calculated with a) ReaxFF and b) DFT-PBE.

*i.e.* sc and dia, result from putting less weight on the description of these phases during the force field optimization. In Fig. 1 it is easily seen that the force field qualitatively reproduces the preference of all bulk phases considered. Table 1 summarizes physical constants calculated from the ReaxFF and DFT-PBE equations of state data for the platinum bulk phases using the four-parameter equation of state fit for solids developed by Li *et al.*[83]. Literature values obtained from other methods (the embedded atom method (EAM)[55], modified embedded atom method (MEAM)[84] and the tight binding (TB)[85]), which were explicitly designed to reproduce such bulk material properties, are also presented for the sake of comparison. Focusing on the fcc bulk phase, ReaxFF yields the same value for the cohesive energy as EAM and MEAM. These underestimate the experimental value by a mere 0.07 eV, whereas the DFT-PBE calculations overestimate this value by 0.38 eV. The optimal lattice constant was input as a independent parameter into the EAM and MEAM force field and thus matches the experimental value of 3.92 Å exactly. Although ReaxFF does not have an independent parameter for this quantity, it is able to reproduce the experimental value with an error of only +0.03 Å. This is comparable to the errors obtained using the DFT-PBE (+0.05 Å) and TB (+0.02 Å) methods. The bulk modulus calculated using MEAM matches the experimental value exactly, while EAM shows a minor underestimation. Both ReaxFF and DFT-PBE substantially underestimate the experimental value by 49 and 38 GPa respectively, and TB exceeds the experimental value by 30 GPa. Considering the remaining two calculated material constants for the fcc bulk phase, it is evident that the ReaxFF-calculated melting point of 2078 K yields the best agreement with experiment[89] (2041 K). The DFT-PBE and MEAM methods exceed the experimentally determined melting point by 77 K and 333 K respectively. The linear thermal expansion coefficient is similarly underestimated by both DFT-PBE and ReaxFF, and overestimated by MEAM. ReaxFF reproduces the qualitative trends for the formation energies of the remaining platinum bulk phases relative to the fcc phase quite well. However, ReaxFF is not able to capture the minuscule, experimentally[82] observed difference of 0.03 eV in the cohesive energies between the platinum fcc and hcp bulk phases. In the case of the *c/a* ratio for the hcp phase there is no experimental value for comparison; however, the ratio obtained from ReaxFF (1.44) is smaller than the ratio obtained from MEAM (1.65), resulting in more densely packed structures. The success of the semi-empirical EAM and MEAM potentials in reproducing the bulk properties (lattice constant, cohesive energy and bulk modulus) is not surprising, since they were explicitly trained to reproduce these properties. In contrast our ReaxFF description was not primarily designed to reproduce bulk material properties, but rather to describe chemical reactions. Nevertheless, these results demonstrate that ReaxFF is a valid alternative for modeling bulk material properties as well.

*3.1.1.2 Transferability to low-index surfaces.* Because ReaxFF was trained to describe platinum in the various coordination states involved in the different bulk phases, the force field is able to describe surface platinum states (where lower coordination numbers are present) with minimal further optimization of the Pt-Pt force field parameters. The success of this sort of extension has already been demonstrated in the de-

**Table 2** Calculated surface energies ($\gamma$) for low-index platinum surfaces and energies of formation ($\Delta\gamma_x = \gamma_x - \gamma_{111}$) relative to the (111) surface are reported in $Jm^{-2}$. The experimental value is for polycrystalline platinum (room temperature value extrapolated to 0 K).

| Surface energy | ReaxFF | DFT-PBE | EAM[55] (1986) | MEAM[57] (1992) | TB[85] (1996) | FCD-LMTO-ASA[91] (1998) | FP-KKR[92] (2002) | MEAM[84] (2003) | Exp.[93] |
|---|---|---|---|---|---|---|---|---|---|
| $\gamma_{111}$ | 1.68 | 1.62 | 1.44 | 1.66 | 2.51 | 2.30 | 2.31 | 1.71 | 2.49 |
| $\gamma_{100}$ ($\Delta\gamma_{100}$) | 1.89 (0.21) | 2.02 (0.40) | 1.65 (0.21) | 2.13 (0.47) | 2.83 (0.32) | 2.73 (0.43) | 2.65 (0.34) | 2.29 (0.58) | |
| $\gamma_{110}$ ($\Delta\gamma_{110}$) | 2.02 (0.34) | 2.14 (0.52) | 1.75 (0.31) | 2.17 (0.51) | 2.97 (0.46) | 2.82 (0.52) | 2.91 (0.60) | 2.33 (0.62) | |

**Table 1** Calculated physical constants for bulk platinum phases. Lattice constants ($a$) are reported in Å, cohesive energies ($E_c$) and energies of formation relative to the fcc structure ($\Delta E_c$) are reported in eV, bulk moduli ($B$) in GPa, linear thermal expansion coefficients ($\alpha$) in $10^{-6}K^{-1}$, and melting points in degrees Kelvin. Experimental values from [a]Ref[86], [b]Ref[87](293.15 K), [c]Ref[88], [d]Ref[89](300 K), and [e]Ref[82] correspond to absolute zero if the temperature is not explicitly given in parenthesis. *The $c/a$ ratio in the DFT-PBE calculations was not optimized but rather assumed to be ideal.

| | | ReaxFF | DFT -PBE | EAM[55] (1986) | TB[85] (1996) | MEAM[84] (2003) | Exp. |
|---|---|---|---|---|---|---|---|
| fcc | $a$ | 3.95 | 3.97 | 3.92 | 3.90 | 3.92 | 3.92[a] |
| | $E_c$ | 5.77 | 6.24 | 5.77 | - | 5.77 | 5.84[a] |
| | $B$ | 239 | 250 | 283 | 318 | 288 | 228[b],288[c] |
| | $\alpha$ | 7.47 | 7.52 | - | - | 9.20 | 8.80[d] |
| | $T_m$ | 2078 | 2118 | - | - | 2374 | 2041[d] |
| bcc | $a$ | 3.13 | 3.16 | - | - | 3.09 | |
| | $E_c$ | 5.65 | 6.24 | - | - | 5.49 | |
| | $B$ | 223 | 249 | - | - | - | |
| | $\Delta E_c$ | 0.12 | 0.00 | - | 0.13 | 0.28 | 0.16[e] |
| sc | $a$ | 2.75 | 2.62 | - | - | 2.60 | |
| | $E_c$ | 4.53 | 5.80 | - | - | 5.01 | |
| | $B$ | 83 | 186 | - | | - | |
| | $\Delta E_c$ | 1.24 | 0.44 | - | 1.07 | 0.76 | |
| $\beta$W | $a$ | 4.96 | 5.05 | - | - | - | |
| | $E_c$ | 5.65 | 6.06 | - | - | - | |
| | $B$ | 225 | 243 | - | - | - | |
| | $\Delta E_c$ | 0.12 | 0.17 | - | 0.35 | - | |
| hcp | $a$ | 3.14 | 3.15 | - | - | 3.11 | |
| | $c$ | 5.13 | 5.10* | - | - | 5.13 | |
| | $E_c$ | 5.77 | 6.24 | - | - | 5.75 | |
| | $B$ | 237 | 255 | - | - | - | |
| | $\Delta E_c$ | 0.00 | 0.00 | - | 0.06 | 0.02 | 0.03[e] |
| dia | $a$ | 6.47 | 5.77 | - | - | 5.92 | |
| | $E_c$ | 3.97 | 4.99 | - | - | 4.06 | |
| | $B$ | 42 | 131 | - | - | - | |
| | $\Delta E_c$ | 1.80 | 1.25 | - | 2.30 | 1.71 | |

velopment of a ReaxFF force field describing gold[69]. Here the only platinum structures with surfaces used in the optimization of the Pt-Pt force field parameters were small platinum clusters with up to 35 atoms reported in an earlier DFT study[90]. To validate the applicability of our ReaxFF force field description for platinum surface structures we report surface energies of unreconstructed low Miller-index surfaces, *i.e.* Pt(111), Pt(100) and Pt(110). In the first two columns of values in Tab. 2 we report surface energies obtained from ReaxFF and DFT-PBE calculations, which were carried out using the same parameters as those used in the calculations for force field optimization. Both the absolute and relative surface energies are in good agreement, with the more stable surfaces showing stronger agreement. This was also the case when we considered more and less stable bulk phases of platinum. For the sake of comparison we also report surface energies obtained from experiment and other computational methods. In addition to the methods mentioned previously in section 3.1.1.1 (EAM, MEAM and TB; see Tab. 1) we also report values obtained from a second MEAM potential by Baskes[57], the Green's function based full-potential screened Korringa-Kohn-Rostoker (FP-KKR) method[92], and the full charge density (FCD-LMTO-ASA) method[91]. Under the assumption that polycrystalline platinum is mainly composed of a mixture of (111), (100) and (110) facets, the electronic structure calculations (FCD-LMTO-ASA, FP-KKR, TB) capture the experimentally determined surface energy reasonably well. Our DFT-PBE calculations appear to underestimate the surface energies. Our ReaxFF force field does the same, as do the other semi-empirical potentials. All methods qualitatively reproduce the generally agreed upon thermodynamic stability sequence for *fcc* metals in vacuum, *i.e.* (111) > (100) > (110). It should be pointed out, that although surface energies were not explicitly included in the ReaxFF parametrization, surface energies obtained from ReaxFF are in qualitative agreement with experimental observations and results from the other computational methods. Hence our Pt-Pt force field description could be successfully applied to study a wide range of platinum systems, just as a comparable ReaxFF description of gold[69] has been fruitfully applied to study phenomena such as diffusion of ad-atoms on low-index surfaces and defects, the stability and morphology of molecular clusters and nanoparticles and even the elongation and rupture of nanowires[94].

### 3.1.2 Training of Pt-O interactions.

*3.1.2.1 Bulk $Pt_xO_y$ phases.* The Pt-O parameters were obtained by optimizing them so that the equations of state of various bulk platinum-oxide phases, *i.e.* $\alpha$-$PtO_2$, $\beta$-$PtO_2$, PtO and $Pt_3O_4$ (see Fig. 2) are accurately described by ReaxFF. Table 3 summarizes the crystallographic parameters and formation energies for these bulk oxides, as measured experimentally, as computed with DFT-PBE[95] and as reproduced by our ReaxFF force field after optimization. Because the potential energy surfaces obtained using our force field for the platinum oxides were relatively flat with multiple local minima, care was taken to perform structural optimization in such a way that the minimized structures resembled the DFT and experimental structures. The force field is able to reproduce the lattice vectors of these oxides within $< 0.2$ Å. The energies of formation were calculated using (Eq. 4):

$$\Delta_f E = \frac{1}{y}\left(E_{Pt_xO_y} - xE_{Pt}^{bulk} - \frac{y}{2}(E_{O_2}^{gas} + E_{O_2}^{ZPE})\right), \qquad (4)$$

where $E_{Pt_xO_y}$ is the total binding energy of the bulk platinum oxide phase, $E_{Pt}^{bulk}$ is the cohesive energy of fcc bulk platinum, $E_{O_2}^{gas}$ is the total energy of a $O_2$ gas-phase molecule ($-5.60$ eV; the O-O parameters are taken from[102,103]), and $E_{O_2}^{ZPE}$ (as calculated within the harmonic approximation, *i.e.* 639.16 $cm^{-1}$; exp.[104] 787.38 $cm^{-1}$) is the zero point energy correction. The $\alpha$-$PtO_2$ is the most stable bulk platinum oxide phase in both DFT-PBE[95] ($-0.72$ eV) and ReaxFF ($-0.64$ eV) calculations. The experimental value[101] ($-0.69$ eV) lies between these DFT-PBE and ReaxFF results. Both experimental measurements[101] ($-0.69$ eV) and DFT calculations[95] find the $\beta$-$PtO_2$ ($-0.72$ eV) structure to be equally stable to the $\alpha$-$PtO_2$. Unfortunately, the ReaxFF force field underestimates the stability of the $\beta$-$PtO_2$ phase by 0.24 eV per oxygen atom under the assumption that the $\alpha$ and $\beta$ phases are equally stable. ReaxFF is able to well reproduce the stability of the bulk PtO phase ($\Delta_f E = -0.50$ eV) as computed with DFT-PBE[95] ($\Delta_f E = -0.49$ eV). The quantitative agreement for the PtO phase can be explained by the presence of surface oxide structures which resemble the bulk PtO phase in the training set used for optimization (see section 3.1.2.2 for details). The largest deviation is encountered in the case of the bulk $Pt_3O_4$ phase ($\Delta_f E = -0.25$ eV for ReaxFF; $\Delta_f E = -0.68$ eV for DFT-PBE[95]). It is not surprising that our ReaxFF force field description underestimates the stabilities of the $\beta$-$PtO_2$ and $Pt_3O_4$ phases, because our parameter optimization focused on the $\alpha$-$PtO_2$ and PtO phases. Indeed, surface oxides on low-index platinum surfaces are known to resemble these two bulk phases[105]. Nevertheless, the most important structural features of all four bulk oxide phases are well described by our force field. Furthermore, because the thermodynamic stabilities of the two critical phases are captured almost exactly the force field should be suitable for investigating bulk oxide formation, low-index oxide surfaces and oxide thin films on low-index platinum surfaces.

*3.1.2.2 O adsorption and absorption on Pt(111).* In addition to the bulk $Pt_xO_y$ phases, adsorbates on Pt(111) and Pt(111) surface oxides were used in the optimization of the Pt-O parameters. Target values for oxygen binding energies (referenced to gas phase $O_2$, without including the zero point energy correction) at high-symmetry adsorption sites (*i.e.* fcc, hcp, top and bridge site) on Pt(111) were taken from previously published DFT cluster calculations[106]. A more detailed discussion of adsorption at these high-symmetry sites can be found in section 3.2. Additional periodic DFT-PBE calculations were performed on $p(3 \times 3)$, $p(2 \times 2)$, $(\sqrt{3} \times \sqrt{3})$R30, and $p(2 \times 1)$ overlayer structures to quantify the influence of coverage dependance on the binding energy of fcc-adsorbed oxygen at coverages between 0.11 ML to 0.50 ML (Fig. 3c) (a)-(d)), where a monolayer (ML) is defined as the ratio between the number of adsorbates and the number of substrate atoms in the top surface layer. As can be seen in Tab. 4, the binding energies per oxygen atom for these structures as calculated using the optimized ReaxFF force field agree with the corresponding target binding energies calculated with DFT-PBE. Both sets of binding energies are in good agreement with other published theoretical values[45,46,107]. Both ReaxFF and DFT-PBE find that the oxygen atoms in the $p(2 \times 2)$ overlayer, corresponding to 0.25 ML, adsorb most strongly to the surface. The energetic preference for this overlayer is more pronounced in the ReaxFF calculations than in the DFT-PBE results. The existence of an energetically optimal surface coverage is generally attributed to attractive lateral interactions resulting from surface relaxation and local changes in surface electronic structure and bonding, which are able to overcome the Coulombic repulsions between adsorbates in particular overlayer structures[108]. To better facilitate comparison between surfaces with different oxygen coverages, we calculated the surface free energies as a function of the chemical potential of oxygen (as determined by its temperature and partial pressure) for four oxygen overlayers (Fig. 3 c) (a)-(d)) and two Pt(111) surface oxides (Fig. 3 c) (e)-(f)) within the *ab-initio* thermodynamics approach[110–113]. The results from ReaxFF and DFT-PBE are summarized in Tab. 4 and presented in Fig. 3. The oxygen chemical potential, which can be expressed in terms of the temperature and partial pressure of oxygen, as evident in the temperature scales, corresponding to UHV ($10^{-13}$ atm) and to ambient (1 atm) conditions, given at the top of Fig. 3, is referenced to $O_{2(g)}$ at 0 K (including the zero point energy). Knowing the relative stabilities of these phases under typical environmental conditions is vital for understanding the chemical nature of the surface. Thus it is essential for ReaxFF to accurately describe the stabilities of these surface phases.

**Table 3** Comparison of structural parameters for bulk platinum oxide phases, obtained from ReaxFF, DFT-PBE and experiments. The parameters include the space group, lattice vector lengths ($a$, $b$, and $c$ reported in Å) and angles between the lattice vectors ($\alpha, \beta$, and $\gamma$ reported in °). The energies of formation ($\Delta_f E$) are reported in eV per oxygen atom and referenced to bulk platinum and molecular oxygen.

| System | Space group | Crystal structure | | | | | | $\Delta_f E$ | | | |
|---|---|---|---|---|---|---|---|---|---|---|---|
| | | ReaxFF | | DFT-PBE[95] | | Exp.[96–99] | | ReaxFF | DFT-PBE[95] | DFT[100] | Exp.[101] |
| $\alpha$-$PtO_2$ | *P-3m1* | a = 3.160 | $\alpha = 90$ | a = 3.153 | $\alpha = 90$ | a = 3.100 | $\alpha = 90$ | −0.64 | −0.72 | −0.62 | −0.69 |
| | | b = 3.160 | $\beta = 90$ | b = 3.153 | $\beta = 90$ | b = 3.100 | $\beta = 90$ | | | | |
| | | c = 4.755 | $\gamma$ =120 | c = 4.545 | $\gamma = 120$ | c = 4.161 | $\gamma = 120$ | | | | |
| $\beta$-$PtO_2$ | *Pnnm* | a = 4.584 | $\alpha = 90$ | a = 4.631 | $\alpha = 90$ | a = 4.484 | $\alpha = 90$ | −0.40 | −0.72 | −0.64 | −0.69 |
| | | b = 4.639 | $\beta = 90$ | b = 4.523 | $\beta = 90$ | b = 4.539 | $\beta = 90$ | | | | |
| | | c = 3.236 | $\gamma = 90$ | c = 3.193 | $\gamma = 90$ | c = 3.136 | $\gamma = 90$ | | | | |
| PtO | *P42/mmc* | a = 3.255 | $\alpha = 90$ | a = 3.133 | $\alpha = 90$ | a = 3.043 | $\alpha = 90$ | −0.50 | −0.49 | −0.41 | |
| | | b = 3.255 | $\beta = 90$ | b = 3.133 | $\beta = 90$ | b = 3.043 | $\beta = 90$ | | | | |
| | | c = 5.334 | $\gamma = 90$ | c = 5.450 | $\gamma = 90$ | c = 5.345 | $\gamma = 90$ | | | | |
| $Pt_3O_4$ | *Pm-3n* | a = 5.712 | $\alpha = 90$ | a = 5.678 | $\alpha = 90$ | a = 5.585 | $\alpha = 90$ | −0.25 | −0.68 | | |
| | | b = 5.712 | $\beta = 90$ | b = 5.678 | $\beta = 90$ | b = 5.585 | $\beta = 90$ | | | | |
| | | c = 5.712 | $\gamma = 90$ | c = 5.678 | $\gamma = 90$ | c = 5.585 | $\gamma = 90$ | | | | |

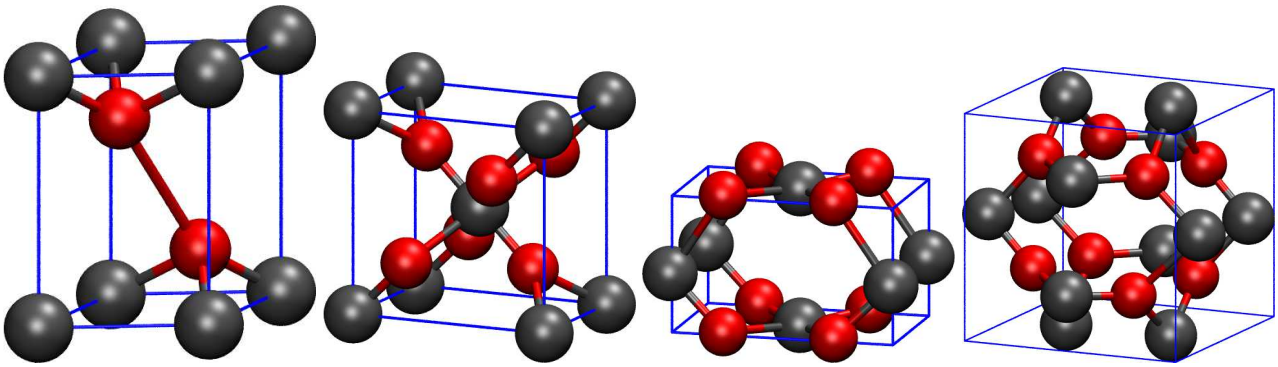

(a) $\alpha$-$PtO_2$ (b) $\beta$-$PtO_2$ (c) PtO (d) $Pt_3O_4$

**Fig. 2** ReaxFF optimized crystal structures of various bulk $Pt_xO_y$ phases. Gray spheres represent platinum atoms; red spheres represent oxygen atoms.

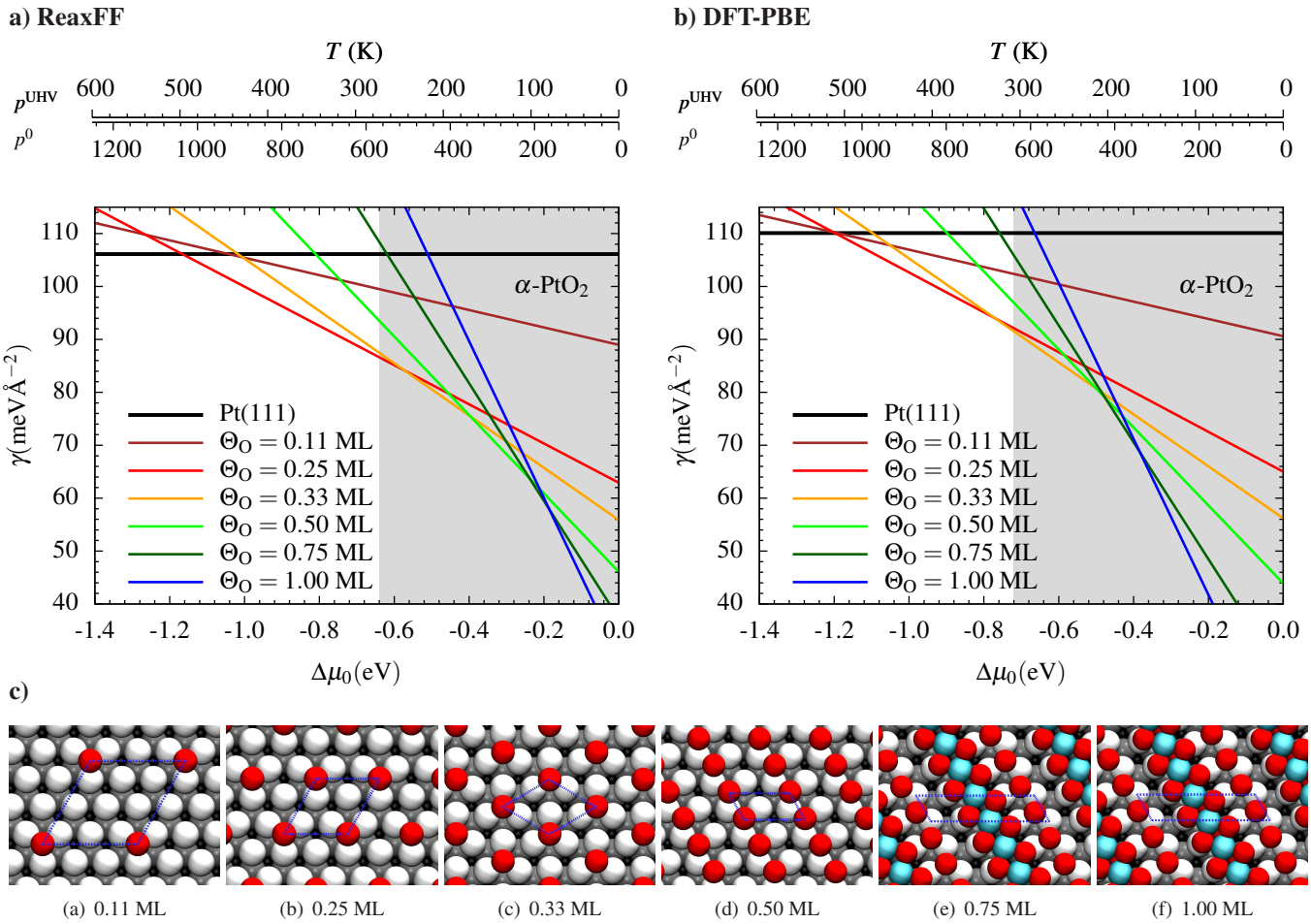


**Fig. 3** Phase diagram for the Pt(111) surface oxidation as a function of the oxygen chemical potential, $\Delta\mu_O$ (where $\Delta\mu_O$ is referred to $O_{2(g)}$ at 0 K) based on a) ReaxFF and b) DFT-PBE. Temperature scales in degrees Kelvin for values of $\Delta\mu_O$ at oxygen partial pressures $p(O_2)$ corresponding to UHV ($10^{-13}$ atm) and standard (1 atm) conditions are given at the very top. The considered oxygen overlayers: (a)-(d) with their respective surface unit cells (dashed blue lines) as well as the minimum surface unit cells of the surface oxide structures: (e)-(f) are illustrated in c). Oxygen atoms are red; platinum atoms are various shades of gray, depending on which layer they belong to and light blue when buckled.

**Table 4** Calculated properties for oxygen overlayers on Pt(111) and Pt(111) surface oxides. Oxygen binding energies per atom ($E_{\mathrm{bind,O}}$) are referenced to gas-phase molecular oxygen and are reported in eV; phase stability ranges (PSR) are in eV and indicate the oxygen chemical potential range the corresponding phase is stable; finally, $\gamma(0)$ is the extrapolated surface free energy for $\Delta\mu_{\mathrm{O}} = 0$ eV. DFT values are taken from Ref [109].

| Method | $\Theta_{\mathrm{O}}$ (ML) | $E_{\mathrm{bind,O}}$ | PSR | $\gamma(0)$ |
|---|---|---|---|---|
| ReaxFF | 0.00 | | $< -1.17$ | 106 |
| | 0.11 | $-1.04$ | - | 89 |
| | 0.25 | $-1.17$ | $-1.17$ to $-0.57$ | 63 |
| | 0.33 | $-1.02$ | $-0.57$ to $-0.40$ | 56 |
| | 0.50 | $-0.81$ | $-0.40$ to $-0.24$ | 46 |
| | 0.75 | $-0.62$ | $-0.24$ to $-0.19$ | 37 |
| | 1.00 | $-0.51$ | $> -0.19$ | 30 |
| DFT-PBE | 0.00 | | $< -1.20$ | 110 |
| | 0.11 | $-1.19$ | - | 91 |
| | 0.25 | $-1.20$ | $-1.20$ to $-0.77$ | 65 |
| | 0.33 | $-1.09$ | $-0.77$ to $-0.50$ | 56 |
| | 0.50 | $-0.91$ | $-0.50$ to $-0.48$ | 44 |
| | 0.75 | $-0.76$ | $-0.48$ to $-0.38$ | 26 |
| | 1.00 | $-0.67$ | $> -0.38$ | 12 |

Indeed, if one takes note of the most stable (*i.e.* lowest free energy) phases over the entire range of chemical potentials, it is easy to see that the DFT-PBE and ReaxFF calculations result in the same stability sequence. However, there are differences of up to 0.2 eV in the chemical potentials at which the transitions between these phases occur, corresponding to temperature discrepancies of up to 100 K under UHV conditions and of up to 200 K under ambient conditions in the temperature scales. That the magnitude of these discrepancies lies primarily on the high sensitivity of the transition temperatures to the binding energies, can be seen by noting the excellent agreement in the binding energies and surface energies at $\Delta\mu_{\mathrm{O}}$=0 in Tab. 4. In any case, ReaxFF gives the same description of the build up of oxygen on Pt(111), in terms of equilibrium phases observed, as the DFT-PBE calculations. Five of these six phases, which both sets of calculations predict to be stable, have been experimentally observed [47,48,114,115], showing that they are stable or, at the very least, metastable surface phases. Indeed, the higher coverage surface phases are metastable in comparison with the bulk $\alpha$-$PtO_2$ phase, as indicated by the shaded regions in Figs. 3 a)-b).

*3.1.2.3 O adsorption on vicinal Pt(111).* Further optimization of the Pt-O parameters involved oxygen adsorbates on monoatomically high steps on Pt(111). The Pt(221) and Pt(335) surfaces were used to model the $\{111\}$ (B-steps) and $\{100\}$-steps (A-steps), respectively. Target values for oxygen binding energies at adsorption sites along these steps (see Fig. 4 b) and c)) were referenced to gas phase $O_2$, without including the zero-point-energy correction and obtained from periodic DFT-PBE calculations [109]. The coverage is given in units of step monolayers (SML), where 1.00 SML corresponds to all fcc sites immediately adjacent to the step, including sites above and below the step, being occupied. As shown in Tab. 5, the oxygen binding energies for these structures, calculated using the optimized ReaxFF force field, generally correlate well with the target values. Adsorption at near-step fcc sites is modestly ($< 0.3$ eV) overestimated by our ReaxFF force field at both types of steps. In contrast, adsorption at bridge sites along the A and B-steps is underestimated by 0.37 eV and 0.27 eV respectively. These opposing trends should be kept in mind for the following discussion. In agreement with DFT calculations performed by Feibelman *et al.* [116], our DFT-PBE calculations predict that the bridge site between highly undercoordinated platinum atoms is the strongest adsorption site for 0.25 SML of oxygen at a $\{100\}$-step (see Fig. 4 c) (1)), with an energetic advantage of 0.34 eV (0.30 eV in Feibelman *et al.*) over the near-step fcc site. ReaxFF underestimates oxygen adsorption at this bridge site by 0.37 eV, with the result that while this site is still stable ($-1.17$ eV), the fcc near-step site (*i.e.* an fcc site directly above the step) is the most stable position ($-1.49$ eV). Turning to $\{111\}$-steps (see Fig. 4 b)), our DFT-PBE calculations, again in agreement with Feibelman *et al.* [116], find that the bridge-site along the step is no longer the most stable adsorption site, since adsorption at a near-step fcc sites is 0.16 eV (0.22 eV by Feibelman *et al.*) more stable. Our ReaxFF force field description reproduces this difference reasonably well with adsorption at a near-step fcc site ($-1.59$ eV) being 0.66 eV more stable than at a bridge-step site ($-0.93$ eV).

The high coverage structures (1.00 SML) on both the A and B-type steps are surface step oxides, and as ReaxFF underestimates the stability of both bulk and surface platinum oxides (see section 3.1.2.1 and 3.1.2.2 respectively) it is not surprising that the stability of these structures are underestimated by ReaxFF as well. Of prime importance for modeling stepped Pt(111) surfaces is the experimental observation that oxygen decorates steps before terraces [117,118]. Our ReaxFF force field description captures this adsorption site preference by successfully reproducing the relative affinities of oxygen for step and terrace sites as calculated using DFT-PBE. Using the procedure described in detail in section 3.1.2.2 the surface free energies were calculated as functions of the oxygen chemical potential for two oxygen overlayers and one Pt(111) surface step oxide for each step-type to better facilitate comparison between stepped surfaces with different oxygen coverages and to help determine the relative stabilities of these phases under typical experimental conditions. In the following we restrict our discussion to comparisons between our ReaxFF and DFT-PBE calculations for each step-type. The relevant results are summarized in Tab. 5 and presented in Fig. 4 a).

In case of the ReaxFF $\{111\}$-step calculations each of the three phases, which correspond to step coverages of 0.25

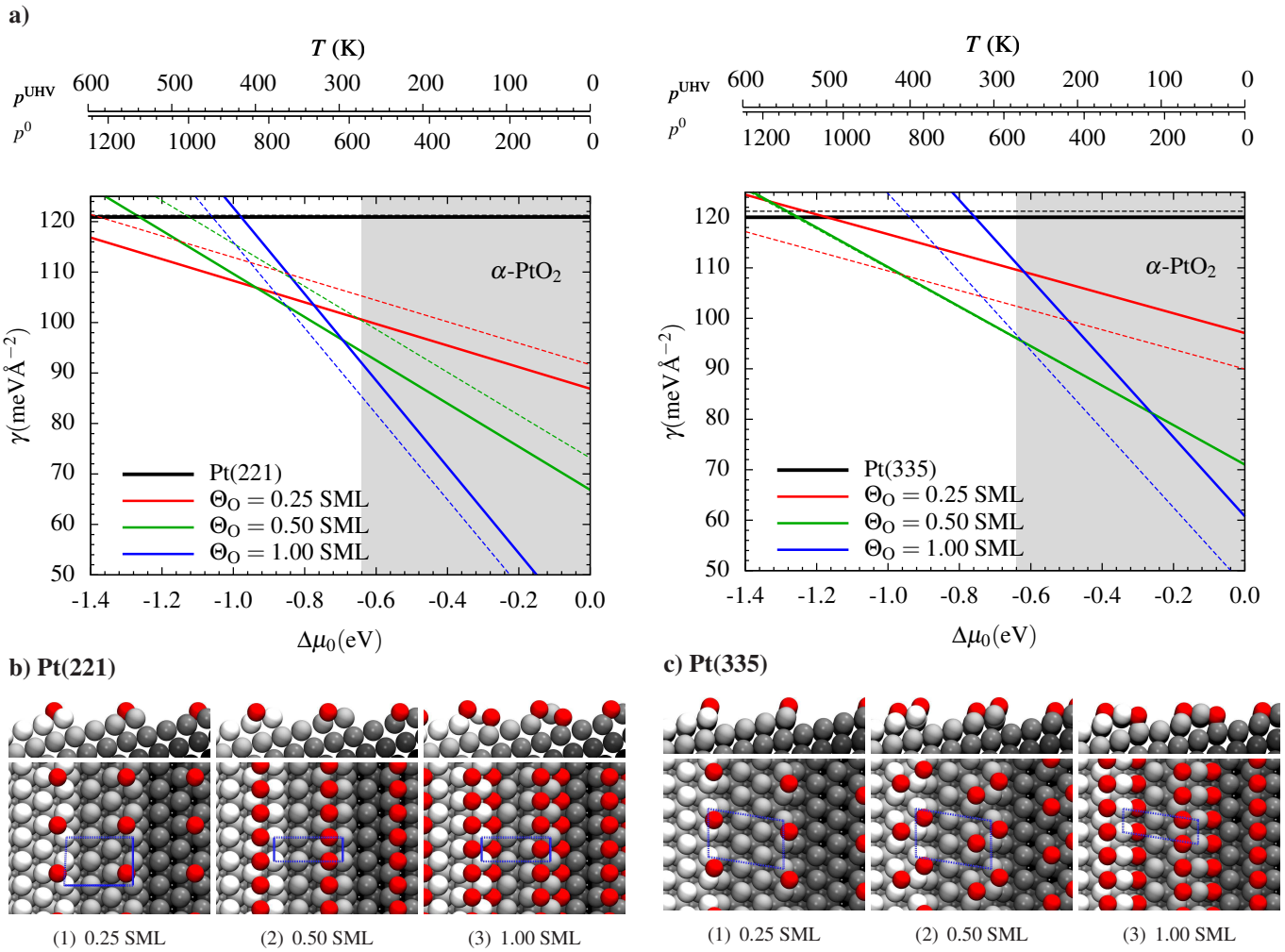


**Fig. 4** ReaxFF and DFT-PBE obtained phase diagrams for the Pt(221) [4(111) × (111)] and the Pt(335) [4(111) × (100)] surface oxidation as a function of the oxygen chemical potential, $\Delta\mu_O$ (where $\Delta\mu_O$ is referred to $O_{2(g)}$ at 0 K) as calculated using ReaxFF (solid lines) and DFT-PBE [109] (dashed lines) are shown in a). Temperature scales in degrees Kelvin for values of $\Delta\mu_O$ at oxygen partial pressures $p(O_2)$ corresponding to UHV ($10^{-13}$ atm) and standard (1 atm) conditions are given at the very top. The considered oxygen overlayers: (1)-(2) with their respective minimum surface unit cells (dashed blue lines) as well as the surface step oxide structure: (3) for each step type are illustrated in b) and c) respectively. Oxygen atoms are red; platinum atoms are various shades of gray, depending on which layer they belong.

SML, 0.50 SML and 1.00 SML, is found to be stable at some oxygen chemical potential between 0 and −1.4 eV. ReaxFF reproduces the surface free energies of all three phases within 6 meVÅ$^{-2}$. In contrast to the two low coverage phases, which are overestimated, the stability of the step oxide phase (1.00 SML) is underestimated as mentioned in the discussion of the binding energies above. This results in the 0.50 SML structure being stable in our ReaxFF force field description for chemical potentials between −0.94 and −0.69 eV, whereas this structure is not stable in the DFT-PBE calculations.

The case of the {100}-step resembles that of the {111}-step insofar as ReaxFF reproduces the surface free energy of the 0.50 SML phase exactly and underestimates the step oxide (1.00 SML) stability by 14 meVÅ$^{-2}$. However, they differ in that the stability of the bridge-site-adsorbed 0.25 SML phase is underestimated by 7 meVÅ$^{-2}$, as has already been mentioned in the discussion of the binding energies, making this phase unstable regardless of the oxygen chemical potential. If we instead consider the lowest energy 0.25 SML phase within our ReaxFF force field description (near-fcc-site-adsorbed oxygen), this coverage becomes stable for chemical potentials between −1.49 and −1.01 eV, since the surface free energy of this phase (as calculated with ReaxFF) matches that of the bridge-site-adsorbed 0.25 SML phase (as calculated with DFT-PBE). Thus, our ReaxFF force field description is nevertheless able to correctly reproduce the chemical-potential-phase-stability window for 0.25 SML of adsorbed oxygen; however, the experimentally observed bridge-site-adsorbed oxygen[116] is not found in the most stable phase until a coverage of 0.50 SML is reached along the {100}-step.

To conclude the discussion of the force field development, we would like to reiterate the extreme sensitivity of the relative surface phase stabilities and transitions between them to minute changes in the oxygen adsorption energies. Nevertheless, we have shown that the ReaxFF force field description developed here correctly reproduces phase diagrams for oxygen adsorption on Pt(111) along with {111} and {100}-steps. This makes this force field description an ideal tool for studying oxidation of a much wider range of platinum surface structures than is possible with DFT calculations. Of immediate interest is filling out the limited computational work, addressing stepped surfaces (with[119–121] or without[15,116] additional defects) to complement experimental work which has been carried out on these systems[117,118,122,123]. Other structures which do not lend themselves as readily to detailed experimental investigation, such as nanoparticles, islands and high-index surfaces also possible subjects of future studies.

**Table 5** Calculated properties for oxygen overlayers on stepped Pt(111) surfaces. The Pt(335) [4(111) × (100)] and Pt(221) [4(111) × (111)] surface orientations were used to model {111} and {100} monoatomic steps respectively. Oxygen binding energies per atom ($E_{\mathrm{bind,O}}$) are referenced to gas-phase molecular oxygen and are reported in eV; phase stability ranges (PSR) are in eV and indicate the oxygen chemical potential range the corresponding phase is stable; finally, $\gamma(0)$ is the extrapolated surface free energy for $\Delta\mu_{\mathrm{O}} = 0$ eV. DFT values are taken from Ref[109].

| Method | Step type | $\Theta_{\mathrm{O}}$ (SML) | $E_{\mathrm{bind,O}}$ | PSR | $\gamma(0)$ |
|---|---|---|---|---|---|
| ReaxFF | {111} | 0.00 | | $< -1.59$ | 121 |
| | | 0.25 | −1.59 | −1.59 to −0.94 | 87 |
| | | 0.50 | −1.26 | −0.94 to −0.69 | 67 |
| | | 1.00 | −0.98 | $> -0.69$ | 37 |
| | {100} | 0.00 | | $< -1.25$ | 120 |
| | | 0.25 | −1.17 | - | 97 |
| | | 0.50 | −1.25 | −1.25 to −0.25 | 71 |
| | | 1.00 | −0.75 | $> -0.25$ | 61 |
| DFT-PBE | {111} | 0.00 | | $< -1.38$ | 121 |
| | | 0.25 | −1.36 | −1.38 to −0.95 | 92 |
| | | 0.50 | −1.13 | - | 73 |
| | | 1.00 | −1.06 | $> -0.95$ | 31 |
| | {100} | 0.00 | | $< -1.61$ | 121 |
| | | 0.25 | −1.54 | −1.61 to −0.97 | 90 |
| | | 0.50 | −1.25 | −0.97 to −0.62 | 71 |
| | | 1.00 | −0.95 | $> -0.62$ | 47 |

### 3.2 PtO force field transferability: further validation & application

Having demonstrated the satisfactory performance of our force field for describing systems used in the optimization, we now validate its transferability to systems it was not explicitly optimized to describe. This aspect of force field validation, the so called transferability test, is an important measure of the quality and reliability of a force field.

**3.2.1 Diffusion-profiles.** As a first step in this direction we consider the diffusion profile of an oxygen atom along a bare Pt(111) surface. The critical points along this profile (*i.e.* fcc, hcp, bridge and top sites) were indeed included in the force field optimization, however, the intermediate points were not. Because a smooth potential energy surface is necessary for conducting physically meaningful MD simulations, it is essential that these intermediate points are correctly described. For this purpose both ReaxFF and DFT nudged elastic band (NEB) calculations were performed on a 4 × 4 unit cell, consisting of 7 layers with the two bottom layers fixed to the bulk lattice distance and a vacuum region of 30 Å. The energy profiles for diffusion between neighboring fcc and hcp sites by traversing either the intermediate bridge ("bridge"-diffusion) or top ("top"-diffusion) site are shown in Fig. 5, where we can see that we indeed have a smooth potential energy surface along the diffusion pathways connecting

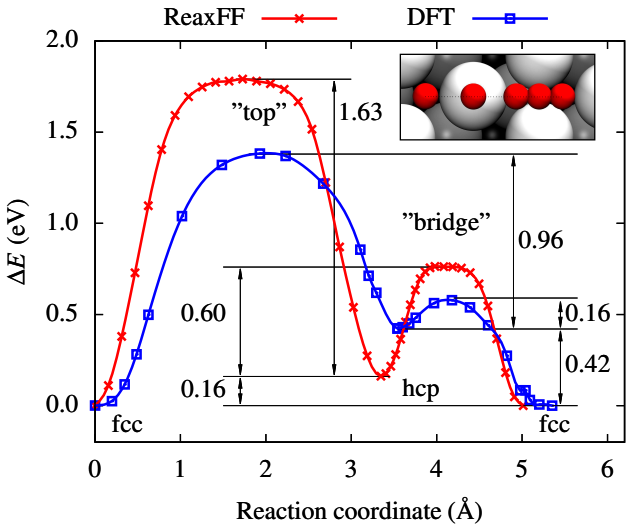


**Fig. 5** Comparison of ReaxFF and DFT-PBE diffusion profiles for an oxygen atom, obtained by means of nudged elastic band (NEB) calculations, for diffusion from an fcc site to a neighboring hcp site by means of an intermediate top site (0-3.5 Å), followed by diffusion to an adjacent fcc site by means of an intermediate bridge site (3.5-5.5 Å). Symbols (squares or crosses) denote calculated data points, solid lines show the fit to the calculated points. In the top right corner an inset figure schematically shows the resting states of oxygen diffusion.

adsorption sites. The small discrepancies in the locations of these adsorption sites along the reaction coordinate are attributable to minor differences in the minimum energy paths, which are nearly identical. Both fcc and hcp sites serve as stable adsorption sites with adsorption at an fcc site being favored by 0.42 eV over adsorption at an hcp site according to DFT-PBE calculations, which are in excellent agreement with other theoretical values (0.40 eV, 0.45 eV)[116,124]. Differentiating adsorption at these two sites is particularly challenging for a force field, because they are identical with the exception of the location of next-nearest neighbors in the subsurface. Nevertheless, our ReaxFF force field description is able to differentiate between fcc and hcp sites, albeit with a smaller difference (0.16 eV) than computed with DFT-PBE (0.42 eV).

Because "bridge"-diffusion is the fastest surface diffusion process, characterizing its transition state is essential for a reliable description of surface processes. Experimentally the energy of this transition state relative to both either an hcp[125] (0.12-0.13 eV) or an fcc[126] (0.43 eV) adsorption, has been deduced from STM studies of $O_2$ dissociation on Pt(111). Our DFT-PBE values for the energy barrier of the "bridge"-diffusion (0.16 eV and 0.58 eV relative to hcp and fcc adsorption respectively) are in reasonably good agreement with these experimental results and DFT calculations performed by Bogicevic *et al.*[124] (0.13 eV and 0.58 eV relative to hcp and fcc adsorption respectively). ReaxFF overestimates the energy of this transition state by 0.18 eV resulting in it lying 0.76 eV and 0.60 eV above fcc and hcp adsorption respectively.

To put the computational speedup provided by ReaxFF into concrete terms we have performed single point energy and force calculations for the starting, final and transition states of "bridge"-diffusion on identical models in SeqQuest (DFT) and ReaxFF. On a single processor the DFT calculations require 136219 s (fcc), 134791 s (bridge) and 139602 s (hcp) and the ReaxFF calculations 26 s (fcc), 28 s (bridge) and 27 s (hcp) for fcc, bridge (TS) and hcp sites respectively. Thus ReaxFF is a factor of $\approx$ 5000 faster than DFT for systems of this size with the calculations settings used throughout this paper.

We are not aware of other studies of "top"-diffusion, but find a DFT-PBE energy barrier of 1.38 eV relative to the initial fcc site. Our ReaxFF force field description overestimates this value by 0.41 eV, leading to it lying 1.79 eV and 1.63 eV above fcc and hcp adsorption, respectively. The overestimation of the energies of these transition states is a side effect of optimizing the force field parameters to differentiate between fcc and hcp adsorption. However, because both barriers are overestimated by similar proportions this should not significantly influence the distribution of diffusion processes sampled in MD simulations. Furthermore, because "bridge"-diffusion is preferred over "top"-diffusion by 1.03 eV in our force field description, regardless of the direction of diffusion (*i.e.* from an fcc to an hcp or vice versa), and DFT-PBE gives analogous results with a difference of 0.80 eV, the statistically anticipated ratios of "bridge" and "top"-diffusion events in ReaxFF can be made to agree exactly with DFT-PBE by appropriately adjusting the temperature. Therefore, our ReaxFF force field description can be reliably used to model the kinetics of O/Pt(111) systems in the context of MD simulations or as the basis for kMC simulations within a multiscale modeling framework[127,128].

#### 3.2.2 Adsorbate displacement within ordered overlayers.

As an example of how our ReaxFF force field can be utilized to study systems which are too complex for routine DFT calculations, we now apply it to study the displacement of individual oxygen atoms from their positions within ordered oxygen overlayers of various oxygen coverages. To isolate the oxygen atom being displaced from its periodic image in adjacent simulation cells, we used large simulations cells, corresponding to a Pt(111) surface seven layers thick with each layer consisting of at least 8×8 platinum atoms (*i.e.* at least 450 atoms per simulation cell!). The $p(4 \times 4)$ ($\Theta_O$= 0.06 ML), $p(3 \times 3)$ ($\Theta_O$= 0.11 ML), $p(2 \times 2)$ ($\Theta_O$= 0.25 ML), ($\sqrt{3} \times$

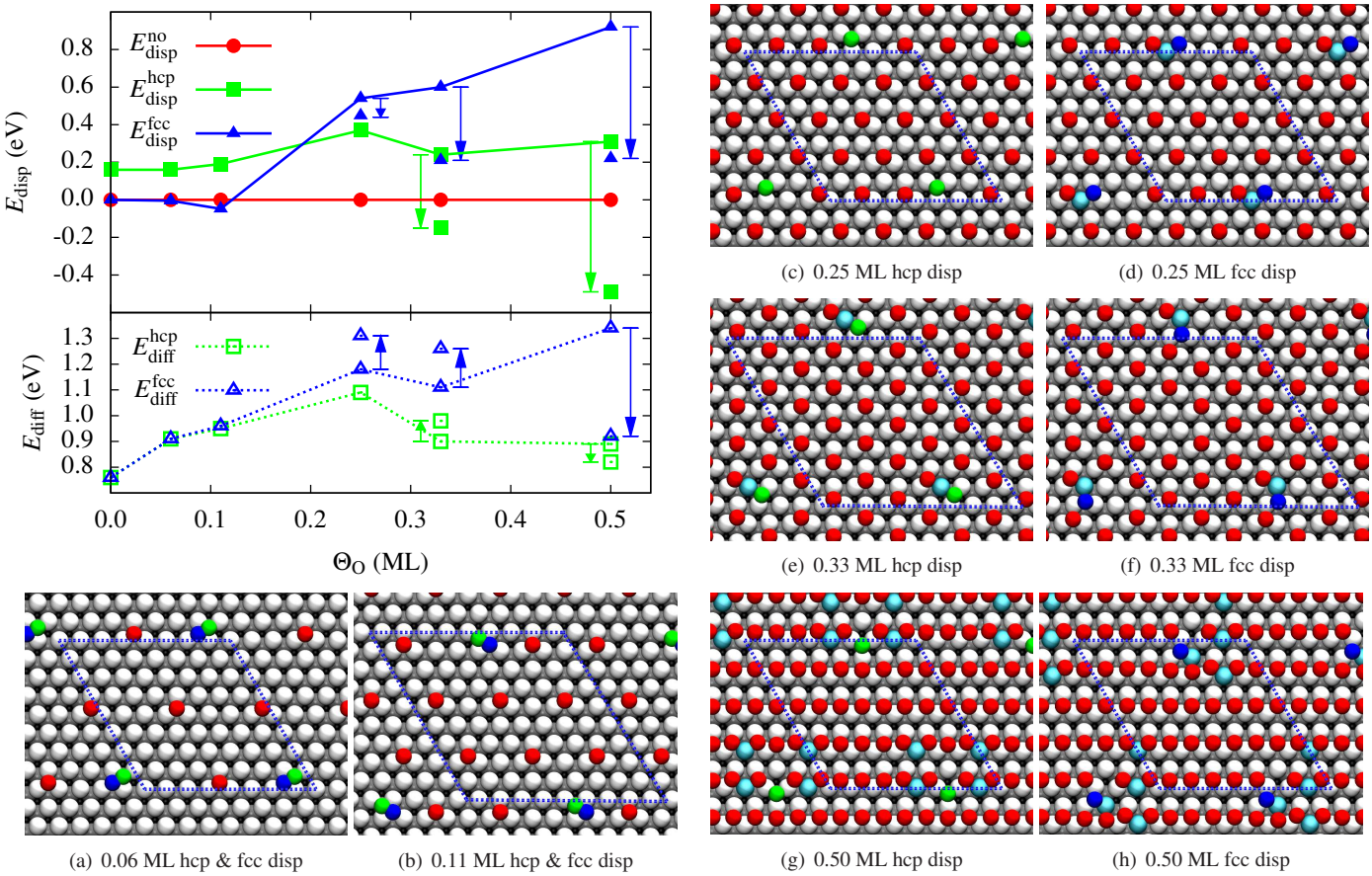


**Fig. 6** Displacement energies ($E_{disp}$) and diffusion barriers ($E_{diff}$) as a function of oxygen coverage ($\Theta_O$). Oxygen overlayers as shown in Fig. 3 are used as starting configurations, from which an O atom is displaced to either an adjacent hcp (green) or fcc (blue) surface site. Dashed lines in the plots denote diffusion barriers, and solid lines denote displacement energies. Top views of displaced structures are shown in images (a)-(h). Undisplaced oxygen atoms are red; the displaced oxygen atom is either green (hcp) or blue (fcc); platinum atoms are various shades of gray, depending on which layer they belong to and light blue when buckled. Dashed lines in the images denote the periodic simulation cell.

$\sqrt{3}$)R30 ($\Theta_O$= 0.33 ML) and $p(2 \times 1)$ ($\Theta_O$= 0.50 ML) overlayers were used as starting configurations. In each of these initial configurations the oxygen atoms are found at fcc sites. A single oxygen atom was displaced across a bridge site to an adjacent hcp site. A second displacement across a bridge site to an adjacent fcc site, sharing a platinum atom with the original fcc site, is also carried out. "Top"-diffusion was not considered, because we had already found it to be less favorable than "bridge"-diffusion. For each displacement we calculated both the energy of the final displaced structure ($E_{disp}$) as well as the barrier associated with the "bridge"-diffusion needed to reach it ($E_{diff}$). The barriers were calculated using the nudged elastic band method and all energies were referenced to the initial overlayer structure. The results are summarized in Fig. 6 as a function of the surface coverage. The first displacement to the adjacent hcp site corresponds to the green data points, where solid lines connect the displacement energies and the dashed lines connect the diffusion barriers. The blue data points and lines correspond to the further displacements to the fcc sites analogously. Given the quantitative discrepancies between DFT-PBE and ReaxFF in computing energies and barriers for oxygen diffusion between fcc and hcp sites (see Fig. 5) we might anticipate that our ReaxFF force field results for surface displacements will tend to be more qualitatively than quantitatively correct. Indeed, we anticipate that the stability at hcp sites is systematically overestimated here along with the diffusion barriers. However, given our ReaxFF force field description's ability to accurately reproduce minute energy differences between various oxygen overlayers, it should even be able to quantitatively account for the additional factors that come into play at these higher coverages. In most cases the displacement of an oxygen atom leads to a higher energy structure. The displacement of an adsorbed oxygen to another fcc site starting from the $p(3 \times 3)$ overlayer is the first exception to this trend, as we observe a weak attraction between oxygen atoms bonded to neighboring platinum atoms without sharing any common platinum neighbors. This weak attraction explains the stability of the $p(2 \times 2)$ overlayer as already discussed in section 3.1.2.2. In the case of displacement to an hcp site only repulsive interactions are observed for coverages below 0.33 ML. Indeed, the closer the displaced oxygen is to another oxygen the stronger the repulsion, as can be observed in the increase of the displacement energy as the coverage increases. For a coverage of 0.25 ML this repulsion can be further increased by displacement to an fcc site, resulting in the oxygen atoms bonding to a common platinum surface atom. The role of repulsion can also be seen in the diffusion barriers at these same coverages ($\Theta_O \leq 0.25$ ML), which increase with increasing surface coverage.

Repulsion plays an even larger role at coverages above 0.25 ML, however the displacements often lead to some interactions being more and some interactions being less repulsive. The displacement of an oxygen to an adjacent hcp site to disrupt the ($\sqrt{3} \times \sqrt{3}$)R30 overlayer leads to a pair of oxygen adsorbates sitting on opposite sites of a shared platinum neighbor. So we expect that this repulsion accounts for about a third of the 0.24 eV associated with the displacement, with the general unfavorability of hcp sites accounting for the rest. If we only consider repulsive interactions, we would anticipate the displacement energy here to be greater than that of the $p(2 \times 2)$ overlayer. However, as already noted, there is an attractive interaction at work in the $p(2 \times 2)$ overlayer, which is lost when a surface atom is displaced. Oxygen atoms with a common platinum neighbor leads to a phenomenon we have not yet discussed, although it was already present in displacement to an fcc site for the $p(2 \times 2)$ overlayer, namely, surface buckling. In surface buckling (indicated by the arrows in the plots in Fig. 6) one or more platinum surface atoms (see the light blue atoms in the images in Fig. 6) move up from the surface plane to separate oxygen atoms which would otherwise be too close to one another, while allowing them to form stronger bonds to the surface. In the case of displacement to an hcp site within the ($\sqrt{3} \times \sqrt{3}$)R30 overlayer a single atom, namely the platinum atom shared by adjacent oxygen atoms, comes out of the surface plane, resulting in an energy relaxation of 0.39 eV. Thus buckling makes this displacement, which results in a local higher coverage, a favorable process ($-0.15$ eV). However, reaching the buckled state requires overcoming a slightly higher barrier (0.98 eV) than arriving at the non-buckled structure (0.90 eV). Further displacement to the next fcc site results in the displaced oxygen atom bonding to two platinum atoms, which are already involved in other Pt-O bonds. One might expect that both platinum atoms with two oxygen neighbors would be pushed out of the surface plane, however, only one of them does. As can be seen in the previous instance, surface buckling results in the oxygen atoms moving away from any neighboring platinum atom that lifts out of the surface plane. This would require that the oxygen atom neighboring both of these platinum atoms be pushed towards the top site above its third platinum neighbor. However, we have already seen that top sites are energetically unfavorable. The alternative is pushing the oxygen in the direction of one of the lower energy bridge sites. In one case this would result in its moving yet closer to one of the other oxygen atoms, which would be energetically unfavorable. In the other case it moves away from both neighboring oxygen atoms, making this the preferred direction for the middle oxygen atom to be pushed in.

In the case of the $p(2 \times 1)$ overlayer, displacing an oxygen atom to an adjacent hcp site increases the number of platinum neighbors it shares with other oxygen atoms from two to three. Albeit the distances to these three oxygen atoms are longer than the distances to the original two were before the displacement. Further displacement to the next fcc site results in all three oxygen oxygen distances (in terms of their

idealized surface sites) returning to their original value. The first of these displacements, breaks up a row of oxygen adsorbates creating space for the two immediate oxygen neighbors to shift toward the vacated site, creating space for their platinum neighbors sitting opposite the bridge sites they have shifted toward to lift out of the surface. The lifting of these platinum atoms enables platinum surface atoms neighboring them to shift toward them, giving the platinum atoms opposite them along the next row of oxygen adsorbates enough space to move away from oxygen atoms above them to lift out of the surface and cause further buckling. This buckling results in an energy gain of 0.8 eV compared to the non-buckled structure, and makes this displacement energetically favorable (−0.49 eV). Furthermore, the barrier for arriving at this buckled structure (0.82 eV) is slightly lower than the barrier for reaching the non-buckled state (0.89 eV). The further displacement of the oxygen atom to the fcc site results in a different buckled state (see Fig. 6 b) (i)) which lies 0.70 eV below the corresponding non-buckled state. Furthermore, the barrier for reaching the buckled state is 0.52 eV lower than the barrier for producing the non-buckled state. Nevertheless, the buckled state is still energetically unfavorable compared with the initial structure before displacement.

With the exception of displacement to form a local $p(2 \times 2)$ overlayer, disrupting these ordered overlayers is found to be energetically unfavorable when surface buckling is not taken into consideration. Surface buckling stabilizes the high coverage structures, however this stabilization is only sufficient in a few cases (displacement to hcp sites) to make the final displaced structure energetically favorable. Furthermore, the barriers for forming these buckled structures are similar to the barrier for oxygen diffusion on a bare Pt(111) surface, making them kinetically accessible. Further details related to the kinetics and atomistic mechanisms involved in forming higher coverage stable surface phases will be addressed in future studies.

**3.2.3 Molecular dynamics simulations of oxygen surface diffusion.** In order to demonstrate the application of our ReaxFF force field to MD simulations, canonical ensemble (NVT) molecular dynamics simulations were performed on an oxygen atom diffusing on a bare Pt(111) surface. The simulations were carried out on a $10 \times 10$ unit cell, consisting of 5 layers with the two bottom layers fixed at their bulk lattice positions and a vacuum region of 30 Å. In order to obtain the diffusion coefficient of an oxygen atom adsorbed on Pt(111), simulations were carried out at five different temperatures: 1800, 2000, 2200, 2300 and 2400 K. These high simulation temperatures enable us to observe a reasonable number of surface diffusion steps within a computationally viable simulation time. Normally one would expect oxygen to desorb as $O_2$ and the platinum surface to melt at these high temperatures. However $O_2$ formation is not possible because there is only one oxygen atom in each periodic simulation cell. Similarly surface melting is not observed for these temperatures at such short time scales. To obtain the temperature-dependent diffusion coefficient for oxygen on Pt(111), the mean square displacement of the oxygen atom was recorded every 12.5 fs (corresponding to every 50 iterations for the 0.25 fs time step used) over the course of the 50 ps simulation at each temperature. The temperature dependent diffusion coefficient for a particle can be extracted from mean square displacements of a function of time with the help of the Einstein relation:

$$D = \lim_{t\to\infty} \frac{1}{2dN_m t} \left\langle \sum_{j=1}^{N_m} [r_j(t) - r_j(0)]^2 \right\rangle \qquad (5)$$

where $d$ is the dimensionality of the system, $t$ the observation time, $N_m$ the total number of simulation atoms and $\langle \sum_{j=1}^{N_m} [r_j(t) - r_j(0)]^2 \rangle$ the ensemble average of the mean square displacement (MSD). This yields diffusion coefficients of $1.05 \cdot 10^{-3}$ cm$^2$ s$^{-1}$, $2.41 \cdot 10^{-3}$ cm$^2$ s$^{-1}$, $1.95 \cdot 10^{-3}$ cm$^2$ s$^{-1}$, $2.56 \cdot 10^{-3}$ cm$^2$ s$^{-1}$ and $4.20 \cdot 10^{-3}$ cm$^2$ s$^{-1}$ at 1800, 2000, 2200, 2300 and 2400 K, respectively. The temperature dependence can be described and separated out by means of an Arrhenius-like relation:

$$D = D_0 \cdot \exp\left(\frac{-E_A}{RT}\right), \qquad (6)$$

where $R$ is the ideal gas constant, $E_A$ the effective activation energy for particle diffusion, $D_0$ the diffusion prefactor and $D$ the diffusion coefficient at a given temperature $T$. This results in a diffusion prefactor ($D_0$) of $1.16 \cdot 10^{-3}$ cm$^2$ s$^{-1}$ and an effective activation energy of 0.68 eV. Given the high temperatures, short time scales, and minimal statistical sampling employed, this effective activation energy agrees extremely well with the "bridge"-diffusion barrier calculated in section 3.2.1 (0.76 eV). Our diffusion prefactor agrees well with other theoretical values ($4.74 \cdot 10^{-3}$, $2.29 \cdot 10^{-3}$ and $1.58 \cdot 10^{-3}$ cm$^2$ s$^{-1}$) reported in the literature[119,129,130]. An experimental value ($\approx 10^{-6.3}$ cm$^2$ s$^{-1}$), which is three orders of magnitude smaller, has also been reported[126]; however the authors reporting it note that it is susceptible to large errors, since it was obtained from data collected within a narrow temperature range. More exotic and ambitious MD simulations making use of our ReaxFF reactive force field are reserved for future reports.

## 4 Conclusions

In this manuscript we report a ReaxFF force field, describing platinum and oxygen in a variety of chemical environments. For the majority of structures and vast majority of low energy structures the ReaxFF potential provides reliable energies and geometries; however there are particular cases where

the force field's reliability is less than desirable (as is the case with any force field). Hence, as always, it is imperitive that the force field be used judiciously and not transfered to new clases of systems without further testing and very possibily additional optimization. Furthermore common sense should be employed in that any improbable or unexpected results should be subject to further testing and validation against other methods before being embraced. The Pt-Pt parameters alone can be utilized to study a wide range of platinum structures including bulk crystalline and amorphous phases, low and high-index surfaces, and nanostructures such as clusters, nanowires and nanotubes. Indeed, not only the chemical properties and atomistic structures of these systems are well described but also their material properties (*e.g.* bulk moduli, linear thermal expansion coefficients).

The Pt-O parameters open up even greater and more numerous opportunities. Because oxygen adsorption on platinum and platinum oxide formation are well described in environments ranging from three-dimensional bulk phases to two-dimensional surfaces to one-dimensional steps, the oxidation of a wide range of platinum structures can be reliably modeled. Furthermore, because the complete spectrum of reasonable oxygen coverages or concentrations was considered for each of these platinum structures, our ReaxFF force field accurately models all stages of the oxidation process in each case. This force field is not only suitable for describing metastable structures but saddle points corresponding to reaction barriers and even provides a smooth potential energy surface for carrying out physically meaningful MD simulations. In considering the high-symmetry diffusion pathways of an oxygen atom along a bare Pt(111) surface, we were able to show that, in spite of overestimating both diffusion barriers, our force field reproduces critical aspects of the kinetics of these processes, in such a way that it could form the basis for MD or kMC simulations. To exhibit the ease with which ReaxFF can be applied to systems beyond the reach of routine DFT calculations, we modeled local displacements of a single oxygen atom from its position in one of five ordered overlayer structures. Of particular interest here is the surface buckling we observed, which leads to highly stable local high-coverage regions for the higher coverage structures. Finally, we displayed the suitability of ReaxFF potential energy surfaces for performing reactive MD simulations by simulating the diffusion of a lone oxygen adatom on Pt(111). From these simulations we were able to extract and derive temperature dependent diffusion coefficients, which could be directly compared with experiments.

## Acknowledgements

The authors thank Stijn Huigh and Erik Neyts for making their Nudged Elastic Band/ReaxFF code available. DF, JB, LS, JEM and TJ thank the financial support from the DFG (Deutsche Forschungsgemeinschaft) and the European Research Council through the ERC-Starting Grant THEOFUN (Grant Agreement No. 259608). JEM gratefully acknowledges support from the Alexander von Humboldt Foundation. ACTvD acknowledges funding from the National Science Foundation Grant No. CBET-1032979.

## References

1 C. Stampfl, H. J. Kreuzer, S. H. Payne, H. Pfnür and M. Scheffler, *Physical Review Letters*, 1999, **83**, 2993–2996.
2 H. Over, Y. D. Kim, A. P. Seitsonen, S. Wendt, E. Lundgren, M. Schmid, P. Varga, A. Morgante and G. Ertl, *Science*, 2000, **287**, 1474–1476.
3 K. Reuter and M. Scheffler, *Physical Review Letters*, 2003, **90**, 046103.
4 R. Blume, M. Hävecker, S. Zafeiratos, D. Teschner, E. Kleimenov, A. Knop-Gericke, R. Schlögl, A. Barinov, P. Dudin and M. Kiskinova, *Journal of Catalysis*, 2006, **239**, 354–361.
5 A. Michaelides, M. L. Bocquet, P. Sautet, A. Alavi and D. A. King, *Chemical Physics Letters*, 2003, **367**, 344–350.
6 J. Schnadt, A. Michaelides, J. Knudsen, R. T. Vang, K. Reuter, E. Lgsgaard, M. Scheffler and F. Besenbacher, *Physical Review Letters*, 2006, **96**, 146101.
7 M. Schmid, A. Reicho, A. Stierle, I. Costina, J. Klikovits, P. Kostelnik, O. Dubay, G. Kresse, J. Gustafson, E. Lundgren, J. N. Andersen, H. Dosch and P. Varga, *Physical Review Letters*, 2006, **96**, 146102.
8 R. Imbihl and J. E. Demuth, *Surface Science*, 1986, 395–410.
9 B. A. Banse and B. E. Koel, *Surface Science*, 1990, **232**, 275–285.
10 E. Lundgren, G. Kresse, C. Klein, M. Borg, J. N. Andersen, M. De Santis, Y. Gauthier, C. Konvicka, M. Schmid and P. Varga, *Physical Review Letters*, 2002, **88**, 246103.
11 M. Todorova, K. Reuter and M. Scheffler, *The Journal of Physical Chemistry B*, 2004, **108**, 14477–14483.
12 B. L. M. Hendriksen and J. W. M. Frenken, *Physical Review Letters*, 2002, **89**, 046101.
13 M. D. Ackermann, T. M. Pedersen, B. L. M. Hendriksen, O. Robach, S. C. Bobaru, I. Popa, C. Quiros, H. Kim, B. Hammer, S. Ferrer and J. W. M. Frenken, *Physical Review Letters*, 2005, **95**, 255505.
14 T. M. Pedersen, W. X. Li and B. Hammer, *Physical Chemistry Chemical Physics*, 2006, **8**, 1566–1574.
15 J. Bandlow, P. Kaghazchi, T. Jacob, C. Papp, B. Tränkenschuh, R. Streber, M. P. A. Lorenz, T. Fuhrmann, R. Denecke and H.-P. Steinrück, *Physical Review B*, 2011, **83**, 174107.
16 T. Matsushima, *Surface Science*, 1983, **127**, 403–423.
17 T. Engel and G. Ertl, *Advances in Catalysis*, Academic Press, 1979, vol. Volume 28, pp. 1–78.
18 R. Adzic, *Electrocatalysis*, Wiley-VCH, 1998.
19 . N. Marković, P. Ross, *Interfacial Electrochemistry: Theory, Experiments and Applications*, Marcel Dekker, 1999.
20 . P. Ross, *Handbook of Fuel Cells: Fundamentals, Technology, Applications*, Wiley-VCH, 2003.
21 A. C. Luntz, J. Grimblot and D. E. Fowler, *Physical Review B*, 1989, **39**, 12903–12906.
22 C. T. Rettner and C. B. Mullins, *The Journal of Chemical Physics*, 1991, **94**, 1626–1635.
23 C. T. Rettner and J. Lee, *The Journal of Chemical Physics*, 1994, **101**, 10185–10188.
24 C. Puglia, A. Nilsson, B. Hernnäs, O. Karis, P. Bennich and N. Mårtensson, *Surface Science*, 1995, **342**, 119–133.
25 A. E. Wiskerke, F. H. Geuzebroek, A. W. Kleyn and B. E. Hayden, *Surface Science*, 1992, **272**, 256–263.

26 X. C. Guo, J. M. Bradley, A. Hopkinson and D. A. King, *Surface Science*, 1994, **310**, 163–182.
27 J. M. Bradley, X.-C. Guo, A. Hopkinson and D. A. King, *The Journal of Chemical Physics*, 1996, **104**, 4283–4293.
28 A. N. Artsyukhovich, V. A. Ukraintsev and I. Harrison, *Surface Science*, 1996, **347**, 303–318.
29 A.-P. Elg, F. Eisert and A. Rosén, *Surface Science*, 1997, **382**, 57–66.
30 A. Eichler and J. Hafner, *Physical Review Letters*, 1997, **79**, 4481–4484.
31 A. V. Walker, B. Klötzer and D. A. King, *The Journal of Chemical Physics*, 1998, **109**, 6879–6888.
32 P. D. Nolan, B. R. Lutz, P. L. Tanaka, J. E. Davis and C. B. Mullins, *The Journal of Chemical Physics*, 1999, **111**, 3696–3704.
33 A. T. Gee and B. E. Hayden, *The Journal of Chemical Physics*, 2000, **113**, 10333–10343.
34 P. Gambardella, v. Šljivančanin, B. Hammer, M. Blanc, K. Kuhnke and K. Kern, *Physical Review Letters*, 2001, **87**, 056103.
35 A. Groß, A. Eichler, J. Hafner, M. J. Mehl and D. A. Papaconstantopoulos, *Surface Science*, 2003, **539**, L542–L548.
36 D. S. Mainardi, S. R. Calvo, A. P. J. Jansen, J. J. Lukkien and P. B. Balbuena, *Chemical Physics Letters*, 2003, **382**, 553–560.
37 K. Stépán, M. Dürr, J. Güdde and U. Höfer, *Surface Science*, 2005, **593**, 54–66.
38 A. Groß, A. Eichler, J. Hafner, M. J. Mehl and D. A. Papaconstantopoulos, *The Journal of Chemical Physics*, 2006, **124**, 174713.
39 C. Sendner and A. Groß, *The Journal of Chemical Physics*, 2007, **127**, 014704.
40 Y. Yokoyama, T. Hori, R. Okada, D. Harimoto, C. Sugawara, Y. Yamada and M. Sasaki, *Surface Science*, 2009, **603**, 2845–2848.
41 D. J. Miller, H. Öberg, L.-Å. Näslund, T. Anniyev, H. Ogasawara, L. G. M. Pettersson and A. Nilsson, *The Journal of Chemical Physics*, 2010, **133**, 224701.
42 P. Valentini, T. E. Schwartzentruber and I. Cozmuta, *The Journal of Chemical Physics*, 2010, **133**, 084703.
43 Y. S. Kim, A. Bostwick, E. Rotenberg, P. N. Ross, S. C. Hong and B. S. Mun, *The Journal of Chemical Physics*, 2010, **133**, 034501.
44 J.-S. McEwen, J. M. Bray, C. Wu and W. F. Schneider, *Physical Chemistry Chemical Physics*, 2012, **14**, 16677–16685.
45 H. Tang, A. Van der Ven and B. L. Trout, *Physical Review B*, 2004, **70**, 045420.
46 R. B. Getman, Y. Xu and W. F. Schneider, *The Journal of Physical Chemistry C*, 2008, **112**, 9559–9572.
47 P. R. Norton, J. A. Davies and T. E. Jackman, *Surface Science*, 1982, **122**, L593–L600.
48 S. P. Devarajan, J. A. Hinojosa Jr. and J. F. Weaver, *Surface Science*, 2008, **602**, 3116–3124.
49 J. M. Hawkins, J. F. Weaver and A. Asthagiri, *Physical Review B*, 2009, **79**, 125434.
50 D. J. Miller, H. Öberg, S. Kaya, H. Sanchez Casalongue, D. Friebel, T. Anniyev, H. Ogasawara, H. Bluhm, L. G. M. Pettersson and A. Nilsson, *Physical Review Letters*, 2011, **107**, 195502.
51 E. F. Holby, J. Greeley and D. Morgan, *The Journal of Physical Chemistry C*, 2012, **116**, 9942–9946.
52 A. C. T. van Duin, S. Dasgupta, F. Lorant and W. A. Goddard, *The Journal of Physical Chemistry A*, 2001, **105**, 9396–9409.
53 M. S. Daw and M. I. Baskes, *Physical Review Letters*, 1983, **50**, 1285.
54 M. S. Daw and M. I. Baskes, *Physical Review B*, 1984, **29**, 6443.
55 S. M. Foiles, M. I. Baskes and M. S. Daw, *Physical Review B*, 1986, **33**, 7983–7991.
56 S. M. Foiles, M. I. Baskes and M. S. Daw, *Physical Review B*, 1988, **37**, 10378.
57 M. I. Baskes, *Physical Review B*, 1992, **46**, 2727–2742.
58 C. J. Casewit, K. S. Colwell and A. K. Rappe, *Journal of the American Chemical Society*, 1992, **114**, 10046–10053.
59 A. K. Rappe, C. J. Casewit, K. S. Colwell, W. A. Goddard and W. M. Skiff, *Journal of the American Chemical Society*, 1992, **114**, 10024–10035.
60 B. R. Brooks, R. E. Bruccoleri, B. D. Olafson, D. J. States, S. Swaminathan and M. Karplus, *Journal of Computational Chemistry*, 1983, **4**, 187–217.
61 W. Damm, A. Frontera, J. Tirado-Rives and W. L. Jorgensen, *Journal of Computational Chemistry*, 1997, **18**, 1955–1970.
62 W. D. Cornell, P. Cieplak, C. I. Bayly, I. R. Gould, K. M. Merz, D. M. Ferguson, D. C. Spellmeyer, T. Fox, J. W. Caldwell and P. A. Kollman, *Journal of the American Chemical Society*, 1995, **117**, 5179–5197.
63 W. D. Cornell, P. Cieplak, C. I. Bayly, I. R. Gould, K. M. Merz, D. M. Ferguson, D. C. Spellmeyer, T. Fox, J. W. Caldwell and P. A. Kollman, *Journal of the American Chemical Society*, 1996, **118**, 2309.
64 J. Tersoff, *Physical Review B*, 1989, **39**, 5566.
65 D. W. Brenner, *Physical Review B*, 1990, **42**, 9458.
66 L. Pauling, *Journal of the American Chemical Society*, 1947, **69**, 542–553.
67 W. J. Mortier, S. K. Ghosh and S. Shankar, *Journal of the American Chemical Society*, 1986, **108**, 4315–4320.
68 T. T. Järvi, A. Kuronen, M. Hakala, K. Nordlund, A. C. T. v. Duin, W. A. G. Iii and T. Jacob, *The European Physical Journal B*, 2008, **66**, 75–79.
69 J. A. Keith, D. Fantauzzi, T. Jacob and A. C. T. van Duin, *Physical Review B*, 2010, **81**, 235404.
70 J. E. Mueller, A. C. T. van Duin and W. A. Goddard, *The Journal of Physical Chemistry C*, 2010, **114**, 4939–4949.
71 Q. Zhang, T. Çağin, A. van Duin, W. A. Goddard, Y. Qi and L. G. Hector, *Physical Review B*, 2004, **69**, 045423.
72 D. Raymand, A. C. van Duin, M. Baudin and K. Hermansson, *Surface Science*, 2008, **602**, 1020 – 1031.
73 K. Joshi, A. C. T. v. Duin and T. Jacob, *Journal of Materials Chemistry*, 2010, **20**, 10431–10437.
74 A. C. T. van Duin, V. S. Bryantsev, M. S. Diallo, W. A. Goddard, O. Rahaman, D. J. Doren, D. Raymand and K. Hermansson, *The Journal of Physical Chemistry A*, 2010, **114**, 9507–9514.
75 T. P. Senftle, R. J. Meyer, M. J. Janik and A. C. T. v. Duin, *The Journal of Chemical Physics*, 2013, **139**, 044109.
76 A. C. T. van Duin, J. M. A. Baas and B. van de Graaf, *Journal of the Chemical Society, Faraday Transactions*, 1994, **90**, 2881.
77 P. J. Feibelman, *Physical Review B*, 1987, **35**, 2626–2646.
78 C. Verdozzi, P. Schultz, R. Wu, A. Edwards and N. Kioussis, *Physical Review B*, 2002, **66**, 125408.
79 J. P. Perdew, K. Burke and M. Ernzerhof, *Physical Review Letters*, 1996, **77**, 3865–3868.
80 D. R. Hamann, *Physical Review B*, 1989, **40**, 2980–2987.
81 S. G. Louie, S. Froyen and M. L. Cohen, *Physical Review B*, 1982, **26**, 1738–1742.
82 A. Dinsdale, *Computer Coupling of Phase Diagrams and Thermochemistry*, 1991, **15**, 317–425.
83 J. H. Li, S. H. Liang, H. B. Guo and B. X. Liu, *Applied Physics Letters*, 2005, **87**, 194111.
84 B.-J. Lee, J.-H. Shim and M. I. Baskes, *Physical Review B*, 2003, **68**, 144112.
85 M. J. Mehl and D. A. Papaconstantopoulos, *Physical Review B*, 1996, **54**, 4519–4530.
86 C. Kittel, *Introduction to solid state physics*, John Wiley & Sons Inc, 1996.
87 G. Kaye and T. Laby, *Tables of physical and chemical constants*, Longman Sc & Tech, 1995.
88 R. Macfarlane, J. Rayne and C. Jones, *Physics Letters*, 1965, **18**, 91–92.

89 D. Lide, *CRC Handbook of Chemistry and Physics, 82nd Edition*, CRC Press, 2001.
90 T. Jacob, R. P. Muller and W. A. Goddard, *The Journal of Physical Chemistry B*, 2003, **107**, 9465–9476.
91 L. Vitos, A. Ruban, H. Skriver and J. Kollár, *Surface Science*, 1998, **411**, 186–202.
92 I. Galanakis, N. Papanikolaou and P. Dederichs, *Surface Science*, 2002, **511**, 1–12.
93 W. Tyson and W. Miller, *Surface Science*, 1977, **62**, 267–276.
94 C. R. Iacovella, W. R. French, B. G. Cook, P. R. C. Kent and P. T. Cummings, *ACS Nano*, 2011, **5**, 10065–10073.
95 T. Jacob, *Journal of Electroanalytical Chemistry*, 2007, **607**, 158–166.
96 R. Hoekstra Henry, S. Siegel and X. Gallagher Francis, *Platinum Group Metals and Compounds*, American Chemical Society, 1971, vol. 98, pp. 39–53.
97 K.-J. Range, F. Rau, U. Klement and A. Heyns, *Materials Research Bulletin*, 1987, **22**, 1541–1547.
98 W. J. Moore and L. Pauling, *Journal of the American Chemical Society*, 1941, **63**, 1392–1394.
99 O. Muller and R. Roy, *Journal of the Less Common Metals*, 1968, **16**, 129–146.
100 W. X. Li, L. Österlund, E. K. Vestergaard, R. T. Vang, J. Matthiesen, T. M. Pedersen, E. L, B. Hammer and F. Besenbacher, *Physical Review Letters*, 2004, **93**, 146104.
101 G. Samsonov, *The Oxide Handbook*, IFI/Plenum, 1973.
102 D. Raymand, A. C. T. van Duin, D. Spngberg, W. A. Goddard III and K. Hermansson, *Surface Science*, 2010, **604**, 741–752.
103 A. C. T. van Duin, C. Zou, K. Joshi, V. Bryantsev and W. A. Goddard, *Computational Catalysis*, The Royal Society of Chemistry, 2014, pp. 223–243.
104 K. K. Irikura, *Journal of Physical and Chemical Reference Data*, 2007, **36**, 389–397.
105 N. Seriani, W. Pompe and L. C. Ciacchi, *The Journal of Physical Chemistry B*, 2006, **110**, 14860–14869.
106 T. Jacob, *Fuel Cells*, 2006, **6**, 159–181.
107 T. Jacob and W. A. Goddard, *ChemPhysChem*, 2006, **7**, 992–1005.
108 P. J. Feibelman, *Annual Review of Physical Chemistry*, 1989, **40**, 261–290.
109 J. Bandlow, *PhD thesis*, Ulm University, 2011.
110 E. Kaxiras, Y. Bar-Yam, J. D. Joannopoulos and K. C. Pandey, *Physical Review B*, 1987, **35**, 9625–9635.
111 G.-X. Qian, R. M. Martin and D. J. Chadi, *Physical Review B*, 1988, **38**, 7649–7663.
112 M. Scheffler and J. Dabrowski, *Philosophical Magazine A*, 1988, **58**, 107–121.
113 K. Reuter and M. Scheffler, *Physical Review B*, 2001, **65**, 035406.
114 H. Steininger, S. Lehwald and H. Ibach, *Surface Science*, 1982, **123**, 1–17.
115 J. F. Weaver, J.-J. Chen and A. L. Gerrard, *Surface Science*, 2005, **592**, 83–103.
116 P. J. Feibelman, S. Esch and T. Michely, *Physical Review Letters*, 1996, **77**, 2257–2260.
117 J. L. Gland and V. N. Korchak, *Surface Science*, 1978, **75**, 733–750.
118 H. Wang, R. G. Tobin, D. K. Lambert, C. L. DiMaggio and G. B. Fisher, *Surface Science*, 1997, **372**, 267–278.
119 J. M. Bray and W. F. Schneider, *Langmuir*, 2011, **27**, 8177–8186.
120 T. Ogawa, A. Kuwabara, C. A. J. Fisher, H. Moriwake and T. Miwa, *The Journal of Physical Chemistry C*, 2013, **117**, 9772–9778.
121 J. M. Bray, J. L. Smith and W. F. Schneider, *Topics in Catalysis*, 2014, **57**, 89–105.
122 J. L. Gland, *Surface Science*, 1980, **93**, 487–514.
123 M. R. McClellan, F. R. McFeely and J. L. Gland, *Surface Science*, 1983, **124**, 188–208.
124 A. Bogicevic, J. Strömquist and B. I. Lundqvist, *Physical Review B*, 1998, **57**, R4289–R4292.
125 B. C. Stipe, M. A. Rezaei, W. Ho, S. Gao, M. Persson and B. I. Lundqvist, *Physical Review Letters*, 1997, **78**, 4410–4413.
126 J. Wintterlin, R. Schuster and G. Ertl, *Physical Review Letters*, 1996, **77**, 123–126.
127 K. Kleiner, A. Comas-Vives, M. Naderian, J. E. Mueller, D. Fantauzzi, M. Mesgar, J. A. Keith, J. Anton and T. Jacob, *Advances in Physical Chemistry*, 2012, **2011**, year.
128 J. E. Mueller, D. Fantauzzi and T. Jacob, in *Multiscale Modeling of Electrochemical Systems*, Wiley-VCH Verlag GmbH & Co. KGaA, 2013, pp. 1–74.
129 S. M. Levine and S. H. Garofalini, *Surface Science*, 1986, **167**, 198–206.
130 J. D. Doll and D. L. Freeman, *Surface Science*, 1983, **134**, 769–776.